Numerical Analysis of the Cylindrical Couette Flow of a Vapor-Gas Mixture

Hiroaki Yoshida and Kazuo Aoki

Department of Mechanical Engineering and Science and Advanced Research Institute of Fluid Science and Engineering, Graduate School of Engineering, Kyoto University, Kyoto 606-8501, Japan

Abstract. A binary mixture of gases confined in a gap between two rotating coaxial circular cylinders is considered. One of the components is assumed to be the vapor of the substance that forms the cylinders, so that it may evaporate or condense (or sublimate) on the cylinder surfaces. The other component is assumed to be a noncondensable gas that neither evaporates nor condenses on the surfaces. Axisymmetric and axially uniform flows (the so-called cylindrical Couette flow) of such a mixture are investigated numerically by the direct simulation Monte Carlo (DSMC) method, with special interest in the near continuum regime. The numerical results demonstrate some interesting effects such as the ghost effect and the flow bifurcation.

Keywords: Boltzmann equation, cylindrical Couette flow, evaporation and condensation, bifurcation
PACS: 51.10.+y, 05.20.Dd, 47.45.-n, 68.03.Fg, 47.20.Ky

INTRODUCTION

Cylindrical Couette flow, which is a textbook example in classical fluid dynamics, is also one of the basic flows for a rarefied gas (see, for example, [1, 2, 3, 4, 5, 6]). The flow is a simple time-independent and spatially one-dimensional flow, and it exhibits neither instability nor bifurcation unless the axial uniformity is released. However, if the gas is a vapor of the substance that forms the cylinders and it undergoes evaporation or condensation (or sublimation) on the cylinders, the situation changes dramatically. The flow exhibits bifurcation for relatively small Knudsen numbers even under the constraint of axial uniformity [7, 8, 9]. In addition, in the fluid-dynamic (or continuum) limit where the Knudsen number goes to zero, the ghost effect [10, 11] manifests itself. More specifically, evaporation and condensation stop in a certain parameter range; however, the infinitesimal evaporation and condensation have a finite effect on the other macroscopic quantities such as the circumferential component of the flow velocity [12].

In the present study, we consider the same problem, i.e., the cylindrical Couette flow of the vapor with evaporation and condensation on the cylinders. The difference from the studies mentioned above is that we consider the case where another gas that neither evaporates nor condenses on the cylinders (noncondensable gas) is also contained between the cylinders. To investigate the present problem, we have performed (i) a numerical simulation using the direct simulation Monte Carlo (DSMC) method [13] for relatively small Knudsen numbers and (ii) a systematic asymptotic analysis for small Knudsen numbers. The results show that some nontrivial effects, such as the ghost effect in the fluid-dynamic limit and flow bifurcation for small Knudsen numbers, manifest themselves. In the present paper, we mainly report on the numerical results of (i), leaving the details of (ii) in a separate paper [14].

PROBLEM AND ASSUMPTIONS

We consider a binary mixture of a vapor (*A*-component) and a noncondensable gas (*B*-component) between two rotating coaxial circular cylinders made of the condensed phase of the vapor. The vapor may undergo evaporation or condensation on the cylinder surfaces, whereas the noncondensable gas neither evaporates nor condenses there. The radius, temperature, and surface velocity of the inner cylinder are denoted by L_I, T_I, and V_I, respectively, and the corresponding quantities of the outer cylinder by L_{II}, T_{II}, and V_{II}. The saturation number density of the vapor molecules at temperature T_I and that at T_{II} are denoted by n_I and n_{II}, respectively. We investigate the steady behavior of the mixture on the basis of kinetic theory under the following assumptions: (i) The behavior of the mixture is described by the Boltzmann equation for hard-sphere molecules; (ii) the molecules of the *A*-component (vapor) leaving the cylinder surfaces are distributed according to the corresponding part of the Maxwellian distribution with n_I, V_I, and T_I (inner cylinder) or n_{II}, V_{II}, and T_{II} (outer cylinder) as the number density, circumferential flow velocity, and temperature; (iii) the molecules of the *B*-component (noncondensable gas) undergo diffuse reflection on the cylinders; (iv) the flow field is axisymmetric and axially uniform.

By the use of appropriate dimensionless variables, we find that the present problem is characterized by the following dimensionless parameters: n_{II}/n_I, n^B_{av}/n_I, T_{II}/T_I, V_I/V_{th}, V_{II}/V_{th}, L_{II}/L_I, m^B/m^A, d^B/d^A, and Knudsen number Kn $(= \ell_I/L_I)$. Here, m^α and d^α are, respectively, the mass and diameter of a molecule of α-component gas ($\alpha = A$ and B); $V_{th} = (2kT_I/m^A)^{1/2}$, where k is the Boltzmann constant, is the most probable speed of the molecules of the A-component in the equilibrium state at rest at temperature T_I; n^B_{av} is the average number density of the B-component over the gap of two cylinders; ℓ_I is the mean free path of the molecules of the A-component in the equilibrium state at rest with number density n_I in the absence of the B-component, i.e., $\ell_I = 1/\sqrt{2}\pi(d^A)^2 n_I$.

We investigate the steady state of the mixture, with special interest in the near continuum (or low Knudsen number) regime, by the DSMC method by Bird [13]. Since the method is a time-dependent one, we obtain the steady solution as the long-time limit of the time-dependent solution of the initial- and boundary-value problem with appropriate initial conditions. We shall describe the initial conditions for the actual computations in the following section.

RESULTS AND DISCUSSION

The solution method employed in this paper is a standard DSMC method [13], so that we omit its description and give only the results. Throughout this section, we let $L_{II}/L_I = 2$, $T_{II}/T_I = 1$, and $V_{II}/V_{th} = 0$ (the outer cylinder is at rest). Since the saturation gas pressure (or number density) is generally a rapidly increasing function of the temperature, it is reasonable to set $T_{II}/T_I = 1$ and $n_{II}/n_I \neq 1$ for the present illustrative discussion.

Effect of vanishing evaporation and condensation

Figures 1 and 2 show the profiles of the macroscopic quantities for $n_{II}/n_I = 2$ (Fig. 1) and $n_{II}/n_I = 0.5$ (Fig. 2) in the case of $V_I/V_{th} = 0.5$, $n^B_{av}/n_I = 0.2$, $m^B/m^A = 0.2$, and $d^B/d^A = 1$. Here, n^A is the molecular number density of the vapor, n^B that of the noncondensable gas, and v_θ, v_r, ρ, and T are, respectively, the tangential component of the flow velocity, the radial component of the flow velocity, the mass density, and the temperature of the entire mixture. In each figure, the results for Kn $= 0.05$, 0.02, 0.01, and 0.005 are shown. The initial condition is IC1 that will be described below (see the first paragraph in the following subsection). In Fig. 1, the vapor evaporates on the outer cylinder and condenses on the inner ($v_r < 0$), whereas in Fig. 2, the opposite takes place ($v_r > 0$). As Kn is decreased, the magnitude of the radial component of the flow velocity ($|v_r|$) decreases and tends to vanish, almost in proportion to Kn, in the continuum limit (Kn $\to 0$). That is, evaporation and condensation tend to stop in the limit. Therefore, we may intuitively think that the flow field should approach the flow field of the ordinary cylindrical Couette flow (of a binary mixture) without evaporation or condensation. However, the other macroscopic quantities in Fig. 1 and those in Fig. 2 approach quite different profiles although evaporation and condensation tend to stop in both cases.

In parallel with the present DSMC computation, we have also performed a systematic asymptotic analysis for small Knudsen numbers on the basis of the Boltzmann equation and derived the correct fluid-dynamic system for the continuum limit [14]. The analysis rigorously shows the following: evaporation and condensation vanish in this limit; however, the infinitesimal evaporation and condensation have a finite effect on the macroscopic quantities. This is an example of the ghost effect (see, e.g., [10, 11]). The profiles of the macroscopic quantities in the continuum limit obtained from the fluid-dynamic system is shown by the solid line. Incidentally, the corresponding profiles in the continuum limit for the ordinary cylindrical Couette flow (i.e., the case where the A-component is also a noncondensable gas) are also shown in the figures by the dashed line. In this case, the saturation number densities n_I and n_{II} have no physical meaning (n_I should be interpreted as a reference number density) and we need to specify the amount of the A-component as well. In Figs. 1 and 2, we have let the total amount of A-component in the case of the dashed line be equal to that in the case of the solid line. In both figures, the DSMC result tends to converge to the asymptotic solutions (solid lines), not to the ordinary cylindrical Couette flow (dashed lines). Depending on the direction of the radial component of the flow velocity vanishing in the continuum limit, the profile of the tangential component v_θ is pushed inward (Fig. 1 where $v_r < 0$) or outward (Fig. 2 where $v_r > 0$) compared to the ordinary cylindrical Couette flow. These features are similar to those of the plane Couette flow of a mixture of a vapor and a noncondensable gas [15].

Flow bifurcation

In this subsection, we investigate the dependence of the steady solution on the initial condition. We use two different initial conditions, that is, IC1: Maxwellian distributions having zero mean velocity, uniform temperature

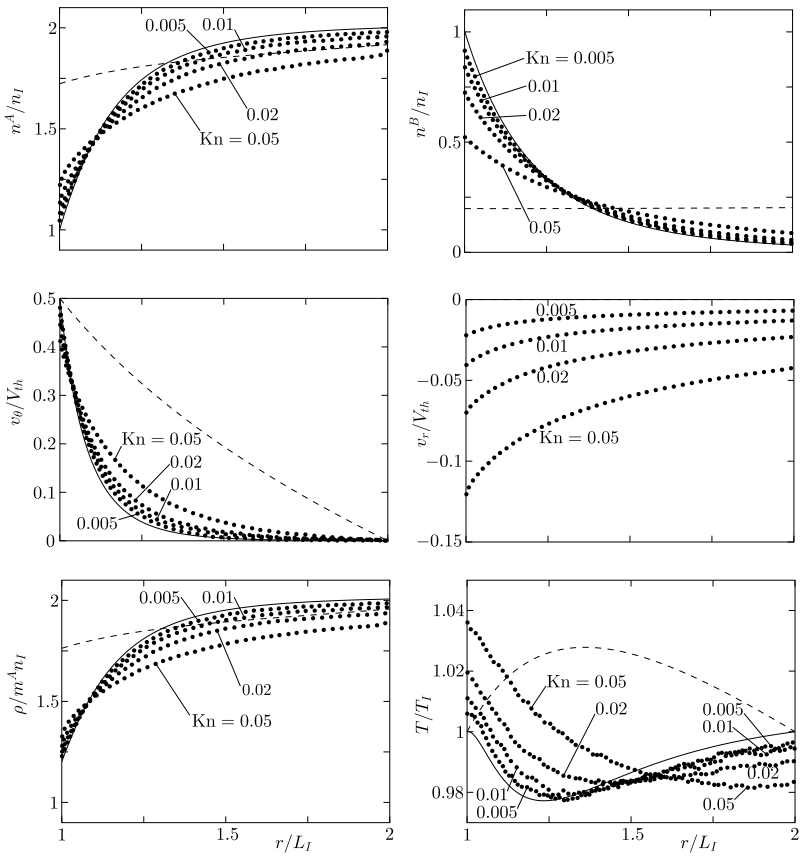

FIGURE 1. Profiles of the macroscopic quantities for small Kn (DSMC result for hard-sphere molecules) in the case of $n_{II}/n_I = 2$, $n^B_{av}/n_I = 0.2$, $V_I/V_{th} = 0.5$, $m^B/m^A = 0.2$, and $d^B/d^A = 1$ ($L_{II}/L_I = 2$, $T_{II}/T_I = 1$, and $V_{II} = 0$). The solid line indicates the profile of the continuum limit, and the dashed line that of the same limit for the ordinary cylindrical Couette flow.

T_I, and uniform number density n_I for A-component and n^B_{av} for B-component; IC2: local Maxwellian distributions corresponding to rigid-body rotation, having angular velocity V_I/L_I, uniform temperature T_I, and number density $n^\alpha = N^\alpha \exp((m^\alpha V_I^2/2kT_I)(r/L_I)^2)$, where $N^\alpha = n^\alpha_0[(L_{II}/L_I)^2 - 1](m^\alpha V_I^2/2kT_I)[\exp((m^\alpha V_I^2/2kT_I)(L_{II}/L_I)^2) - \exp(m^\alpha V_I^2/2kT_I)]^{-1}$ with $n^A_0 = n_I$ and $n^B_0 = n^B_{av}$. In addition to these two, another initial condition has been used for some supplementary computations.

Let us denote by M_r the steady mass flow of the vapor in the radial direction per unit time and per unit length of the axial direction. According to the asymptotic analysis, M_r ($= 2\pi r \rho v_r$) is of the order of Kn and thus vanishes in the continuum limit. Let $\widetilde{M}$ denote the dimensionless mass-flow rate magnified by Kn, i.e., $\widetilde{M} = (2/\sqrt{\pi})(M_r/\mathrm{Kn})[2\pi L_I m^A n^I V_{th}]^{-1}$.

Figure 3(a) shows $\widetilde{M}$ versus the surface velocity of the inner cylinder V_I for Kn = 0.05, 0.02, 0.01, and 0.005 in the case of $n_{II}/n_I = 1.5$, $n^B_{av}/n_I = 0.05$, $m^B/m^A = d^B/d^A = 1$. Since the saturation number density (or pressure) of the vapor on the outer cylinder is higher than that on inner ($n_{II}/n_I = 1.5$), we expect an inward radial mass flow ($\widetilde{M} < 0$), with evaporation on the outer cylinder and condensation on the inner, for small V_I. But for large V_I, the pressure of the vapor near the outer (or inner) cylinder may become higher (or lower) than the saturation pressure there because of the centrifugal force, so that an outward radial mass flow ($\widetilde{M} > 0$), with evaporation on the inner and condensation on the outer, is expected. In fact, for Kn = 0.05 and 0.02, the two different initial conditions IC1 and IC2 give the same solution (within the computational error), and $\widetilde{M}$ increases monotonically with V_I, changing the sign at around $V_I/V_{th} = 1$. For Kn = 0.01, however, $\widetilde{M}$ exhibits a jump from a negative to a positive value at $V_I/V_{th} = 1.03$. That is, there are two solutions at this point: one with $\widetilde{M} < 0$ obtained with IC1 and the other with $\widetilde{M} > 0$ obtained with IC2. For Kn = 0.005, the two families of solutions, one with $\widetilde{M} < 0$ obtained with IC1 and the other with $\widetilde{M} > 0$ obtained with IC2, coexist in the range $0.99 \le V_I/V_{th} \le 1.04$. That is, the solution is not unique in this range, and bifurcation of

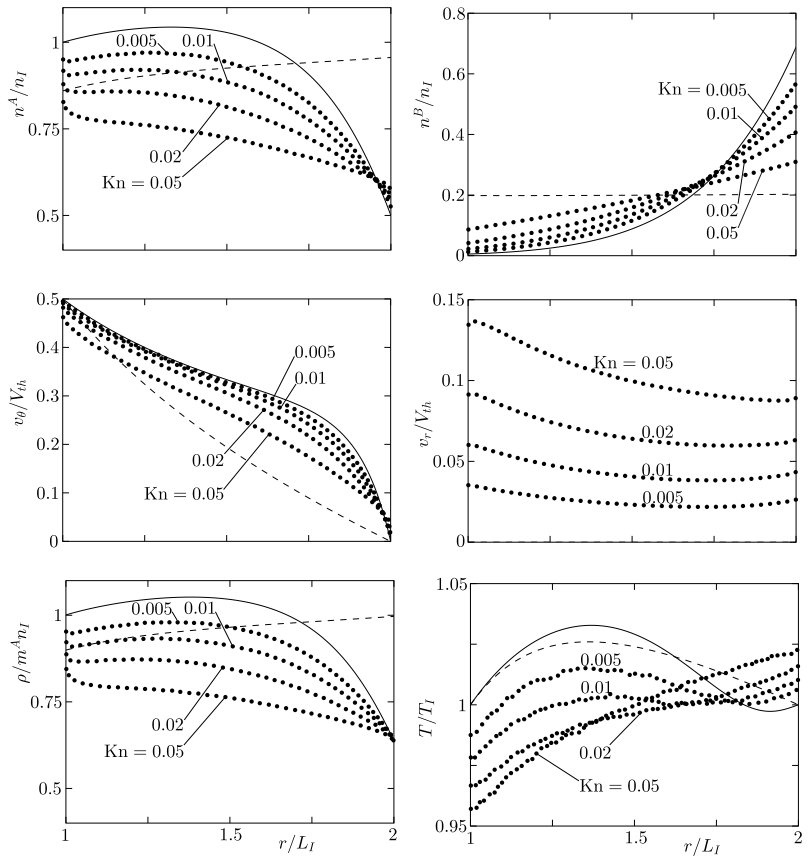

FIGURE 2. Profiles of the macroscopic quantities for small Kn (DSMC result for hard-sphere molecules) in the case of $n_{II}/n_I = 0.5$, $n^B_{av}/n_I = 0.2$, $V_I/V_{th} = 0.5$, $m^B/m^A = 0.2$, and $d^B/d^A = 1$ ($L_{II}/L_I = 2$, $T_{II}/T_I = 1$, and $V_{II} = 0$). See the caption of Fig. 1.

the solution takes place. In Fig. 3(a), the corresponding result in the continuum limit is also shown by the solid line. The curve is of "S" shape and shows the non-uniqueness of the solution in the range $0.9388 \le V_I/V_{th} \le 1.1100$. The DSMC result approaches the curve as Kn decreases. However, our DSMC computation was not able to give solutions that correspond to the part with negative gradient of the curve. We have made some attempts to obtain such a solution, which will be described bellow.

Figure 3(b) shows $\widetilde{M}$ versus V_I for $n^B_{av}/n_I = 0.5$, 0.05, and 0.02 in the case of Kn $= 0.005$, $n_{II}/n_I = 1.5$, and $m^B/m^A = d^B/d^A = 1$ [the plot for $n^B_{av}/n_I = 0.05$ has been already shown in Fig. 3(a)]. For $n^B_{av}/n_I = 0.5$, the solution does not depend on the initial condition, and $\widetilde{M}$ increases monotonically with increasing V_I. Flow bifurcation occurs for smaller n^B_{av}/n_I ($n^B_{av}/n_I = 0.05$ and 0.02). The range of V_I where the bifurcation occurs is wider for smaller n^B_{av}/n_I ($n^B_{av}/n_I = 0.02$). In the figure, the corresponding results in the continuum limit [14] are also shown by the solid line. They form "S" shaped curves, as in Fig. 3(a).

The profiles of the tangential velocity v_θ and the radial velocity v_r at some points in Fig. 3(b) are shown in Fig. 4. More specifically, two different profiles with $\widetilde{M} > 0$ and $\widetilde{M} < 0$ at $V_I/V_{th} = 1.0053$ are shown for $n^B_{av}/n_I = 0.05$ [(a)] and $n^B_{av}/n_I = 0.02$ [(b)] in the case of Kn $= 0.005$, $n_{II}/n_I = 1.5$, and $m^B/m^A = d^B/d^A = 1$. The profiles in the continuum limit for the corresponding parameters are also shown by the solid line. The curve with label $\widetilde{M} = 0$ indicates the profile of the solution at the point $(V_I/V_{th}, \widetilde{M}) = (1.0053, 0)$ (common for all n^B_{av}/n_I) in Fig. 3(b). We note that the solutions at the point $(V_I/V_{th}, \widetilde{M})$= (1.0053, 0) in the continuum limit coincide with the ordinary cylindrical Couette flow in the same limit.

Recall that the solution corresponding to this solution could not be obtained by the DSMC computation. Our attempt to obtain such a solution for Kn $= 0.005$ by the DSMC method is described in the following. We first obtain the solution of the ordinary cylindrical Couette flow (i.e., in the case where both components are noncondensable) at

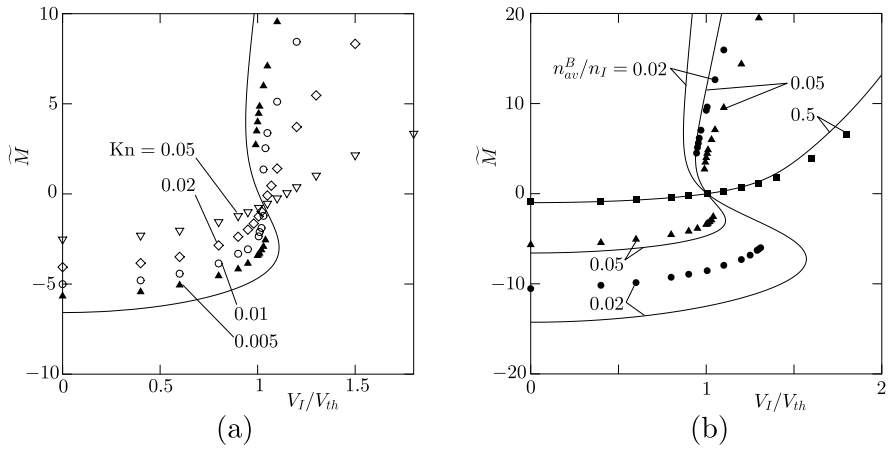

FIGURE 3. Magnified mass flow rate $\widetilde{M}$ versus V_I/V_{th} for $n_{II}/n_I = 1.5$, $m^B/m^A = 1$, and $d^B/d^A = 1$ ($L_{II}/L_I = 2$, $T_{II}/T_I = 1$, and $V_{II} = 0$). (a) $n^B_{av}/n_I = 0.05$ and Kn $= 0.05$ (▽), 0.02 (◇), 0.01 (○), and 0.005 (▲), (b) Kn $= 0.005$ and $n^B_{av}/n_I = 0.5$ (■), 0.05 (▲), and 0.02 (●). The solid line indicates the results in the continuum limit (Kn $\to 0$).

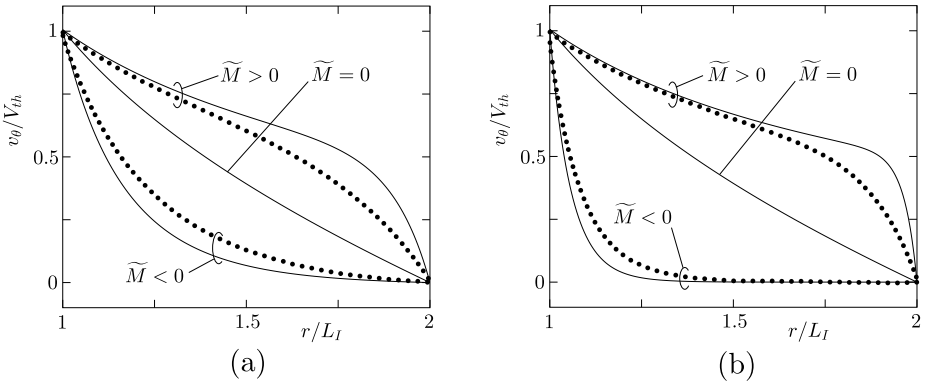

FIGURE 4. Profiles of the tangential velocity v_θ and the radial velocity v_r at Kn $= 0.005$ in the case of $n_{II}/n_I = 1.5$, $V_I/V_{th} = 1.0053$, $m^B/m^A = 1$, and $d^B/d^A = 1$ ($L_{II}/L_I = 2$, $T_{II}/T_I = 1$, and $V_{II} = 0$). (a) $n^B_{av}/n_I = 0.05$, (b) $n^B_{av}/n_I = 0.02$.

$V_I/V_{th} = 1.0053$ for $n^B_{av}/n_I = 0.05$ and 0.02 [see Fig. 3(b)]. In this preliminary computation, we need to specify the total amount of A-component instead of n_{II}/n_I. The amount of A-component is chosen to be equal to that of the solution at (V_I/V_{th}, $\widetilde{M}$)= (1.0053, 0) of the continuum limit. Then, we perform the DSMC computation with these solutions of ordinary cylindrical Couette flow as the initial condition. In both cases of $n^B_{av}/n_I = 0.05$ and 0.02, the solution ended up in the lower branch, i.e., $\widetilde{M} = -3.25$ for $n^B_{av}/n_I = 0.05$ and $\widetilde{M} = -8.53$ for $n^B_{av}/n_I = 0.02$. These initial conditions should be close enough to the solution that we search for. Therefore, it is highly probable that this solution is unstable. (It is noted that the solution of the continuum limit, which has been obtained by a steady scheme from the fluid-dynamic system, can always be obtained regardless of its stability.)

Figure 5 shows $\widetilde{M}$ versus n^B_{av} in the case of $V_I/V_{th} = 1.0053$, Kn $= 0.005$, $n_{II}/n_I = 1.5$, $m^B/m^A = d^B/d^A = 1$. The corresponding curve for the continuum limit is also shown. From this figure, we can see how the solution bifurcates. As can be conjectured from the curve for the continuum limit, the bifurcation is a pitchfork type; the middle solution is most probably unstable (see the previous paragraph).

Remarks on DSMC computation

One may think that the DSMC computation of the present spatially one-dimensional problem is easy. In reality, it is not true because of the structure of the solution. As we have seen, very slow radial velocity v_r has a substantial effect on the entire flow field (ghost effect, see the subsection “Effect of vanishing evaporation and condensation”).

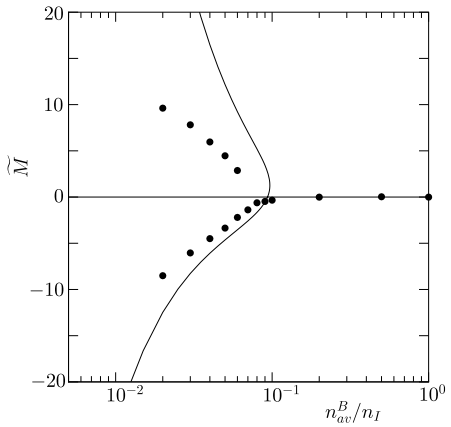

FIGURE 5. Magnified mass flow rate $\widetilde{M}$ versus n^B_{av}/n_I at Kn $= 0.005$ in the case of $n_{II}/n_I = 1.5$, $V_I/V_{th} = 1.0053$, $m^B/m^A = 1$, and $d^B/d^A = 1$ ($L_{II}/L_I = 2$, $T_{II}/T_I = 1$, and $V_{II} = 0$). The solid line indicates the results in the continuum limit.

Therefore, the slow radial velocity should be obtained accurately. Otherwise, other macroscopic quantities cannot be described correctly. As is well known, however, one of the drawbacks of the DSMC method is the difficulty in obtaining small quantities because they are buried in the statistical fluctuations inherent to the method. Since the radial velocity in the present problem vanishes (almost) in proportion to the Knudsen number, the computation becomes increasingly difficult with the decrease of the Knudsen number. This difficulty, which has been pointed out in [15], may be overcome only by a large computational system and a long-time run. In the present computation, the interval $1 \le r/L_I \le 2$ is divided into 400 (Kn $= 0.05$, 0.02, and 0.01) or 800 (Kn $= 0.005$) uniform cells; 200 simulation particles per cell are used for the number density $n^A = n_I$ in Fig. 2, and 100 particles per cell for $n^A = n_I$ in the rest of the figures. The time step Δt is $4.51 \times 10^{-3} t_*$ (Kn $= 0.05$), $5.64 \times 10^{-3} t_*$ (Kn $= 0.02$ and 0.01), or $1.13 \times 10^{-2} t_*$ (Kn $= 0.005$), where t_* is the mean free time corresponding to T_I and ℓ_I. The computation was performed for more than $10^6 \Delta t$ (Kn $= 0.05$), $2 \times 10^6 \Delta t$ (Kn $= 0.02$), or $4 \times 10^6 \Delta t$ (Kn $= 0.01$ and 0.005) after the steady state has been established, and the averages over these time intervals are shown in the figures.

ACKNOWLEDGMENTS

This work is supported by the Grants-in-Aid for Scientific Research (Nos. 17360041 and 16001161) from JSPS and by the Center of Excellence for Research and Education on Complex Functional Mechanical Systems. The junior author (H. Y.) participated in the present work as a JSPS Research Fellow.

REFERENCES

1. Cercignani, C. and Sernagiotto, F., Phys. Fluids **10**, 1200-1204 (1967).
2. Nanbu, K., Phys. Fluids **27**, 2632-2635 (1984).
3. Sharipov, F. and Kremer, G., Transp. Theory Stat. Phys. **25**, 217-229 (1996).
4. de Socio, L. M., Ianiro, N., and Marino, L., J. Thermophys. Heat Transfer **14**, 269-275 (2000).
5. Aoki, K., Yoshida, H., Nakanishi, T., and Garcia, A. L., Phys. Rev. E **68**, 016302 (2003).
6. Yuhong, S., Barber, R. W., and Emerson, D. R., Phys. Fluids **17**, 047102 (2005).
7. Sone, Y., Sugimoto, H., and Aoki, K., Phys. Fluids **11**, 476-490 (1999).
8. Sone, Y. and Doi, T., Phys. Fluids **12**, 2639-2660 (2000).
9. Sone, Y., Handa, M., and Sugimoto, H., Transp. Theory Stat. Phys. **31**, 299-332 (2002).
10. Sone, Y., Aoki, K., Takata, S., Sugimoto, H., and Bobylev, A. V., Phys. Fluids **8**, 628-638 (1996); Erratum: *ibid* **8**, 841 (1996).
11. Sone, Y., *Kinetic Theory and Fluid Dynamics*, Birkhäuser, Boston, 2002.
12. Sone, Y., Takata, S., and Sugimoto, H., Phys. Fluids **8**, 3403-3413 (1996); Erratum: *ibid* **10**, 1239 (1998).
13. Bird, G. A., *Molecular Gas Dynamics*, Oxford University Press, Oxford, 1976; *Molecular Gas Dynamics and the Direct Simulation of Gas Flows*, Oxford University Press, Oxford, 1994.
14. Yoshida, H. and Aoki, K., Phys. Fluids (in press).
15. Takata, S. and Aoki, K., Phys. Fluids **11**, 2743-2756 (1999).